IR NONLINEAR PHOTOTHERMAL RADIOMETRY IN CARBON/EPOXY COMPOSITE MATERIALS: EXPERIMENTAL SURVEY

G.Kalogiannakis[1,*], J. Ravi[2], S. Longuemart[2], E. H. Bentefour[2], D. Van Hemelrijck[1] and C. Glorieux[2]

[1]Department of Mechanics of Materials and Constructions, Vrije Universiteit Brussel, Pleinlaan 2, Belgium
[2]Laboratorium voor Akoestiek en Thermische Fysica (ATF), Department of Physics and Astronomy, K.U.Leuven, Belgium

ABSTRACT

Two different approaches were used to investigate the potential for non-destructive testing of thermal nonlinear effects in composite materials. Second harmonic generation in thermal-wave fields has attracted much attention in recent years for the non-destructive evaluation of solid structures. Even though not the only source, the presence of a defect can result in a strong nonlinear signature, which could enhance the detectability of photothermal methods. The following experimental survey trails several theoretical analyses on the subject, mostly for homogeneous isotropic samples. As composite material structures exhibit often thermo-mechanical nonlinearities originating from the polymer matrix, they appeared to be ideal candidates to exploit the potential of nonlinear photothermal radiometry. In this work, a theoretical model is developed, which could be used to estimate the generated overtones that originate from the most common cause of failure of composites, the delamination. The contribution of other rival but parallel effects is also quantified and compared with the one of interest. Finally, experimental validation with infrared photothermal radiometry demonstrates the reliability of the theoretical assertions.

1. INTRODUCTION

In principle, nonlinear photothermal radiometry exploits higher harmonic signal generation for non-destructive testing. The temperature field imposed by amplitude modulated laser excitation depends on variations in thermal properties [1-3] as well as the synchronous modification of the boundary conditions [4, 5]. Such effects, which are closely linked with the present of a defect, allow enhancing the contrast of a defected area by detecting the second harmonic temperature signal.

The theoretical potential of using nonlinear photothermal radiometry in fibre reinforced composite materials partially emerged as measurements demonstrated recently that the thermal properties exhibit strong dependence on temperature [2, 3]. Nonlinear effects are often present in composites, and originate from the thermomechanical behaviour of the polymer matrix. Numerical analysis using a finite element model of this particular nonlinearity has motivated to perform an experimental examination. When a defect is introduced in an intact sample, spectral analysis shows that the second harmonic of the surface temperature signal is affected much more than the fundamental frequency component. Although the contrast for both signal components follows the same pattern for the fundamental and the second harmonic, the respective relative values are strongly different. This implies in practice a better visibility of the defect.

Moreover, delaminations are very often formed in composites due to large interlaminar shear stresses. Modulated laser excitation alters the uniform temperature field to a gradient with higher temperatures near the surface. Therefore, non-uniform thermal expansion results in thermoelastic bending, the modulation of which imposes a vibration of the layer above the delamination [6] at the excitation frequency. The triggered oscillation of the air gap in the delamination entails an alteration of the boundary condition for the heat diffusion problem. This phenomenon was first accredited to explain the strong nonlinearities observed [7]. Later it was shown theoretically that this effect can be really effective [4].

In this work, a theoretical model is developed to estimate the order of magnitude of the second harmonic that originates from the vibration of a thin composite layer above a delamination. Moreover, different experimental setups were used to investigate the potential that is associated with nonlinear photothermal radiometry in composites. A Laser Vibrometer

method was used to evaluate the displacement field above a delamination and the fundamental thermal-wave field was fitted for different defect thicknesses using a mushroom-like sample. As will be shown, the amplitude and the phase of the second harmonic are approximately equal to the difference of the fundamental components at static conditions for the delamination size. Measurements using infrared radiometry give an experimental estimate of their order of magnitude.

2. THEORETICAL BACKGROUND

The thermal and the displacement-wave fields in a solid are in general coupled through the equations of thermoelastodynamics [8]. These equations are formulated for a homogeneous anisotropic unbounded medium as follows:

$$\begin{aligned} C_{ijkl}u_{k,lj} + f_i &= \rho\ddot{u}_i \\ f_i &= -\beta_{ij}\theta_{ij} \\ \rho C_p\dot{\theta} - k_{ij}\theta_{,ij} + T_0\beta_{ij}\dot{u}_{i,j} &= Q \end{aligned} \tag{1}$$

where Einstein's convention on the indices i, j, k and l is adopted. The displacement field $\boldsymbol{u}$ is a vector-valued function, while the change of temperature θ with respect to a given initial temperature distribution, is a scalar-valued function. In the wave equation, the components of the fourth order tensor $\boldsymbol{C}$ represent the adiabatic elastic constants, ρ is the density and the vector-valued function $\boldsymbol{f}$ consists of the body forces. These forces depend linearly on the temperature field by means of the tensor $\boldsymbol{\beta}$, the components of which depend on the thermal coefficients of linear expansion $\boldsymbol{\alpha}$, as shown in the following equation:

$$\beta_{ij} = C_{ijkl}\alpha_{kl} \tag{2}$$

In the heat diffusion equation, C_p is the specific heat per unit volume at constant pressure and $\boldsymbol{k}$ is the conductivity tensor. In what follows, according to the theory of thermal stresses, the source term $T_0\beta_{ij}\dot{u}_{i,j}$ of thermoelastic origin on the left-hand side has minor contribution and so can be neglected.

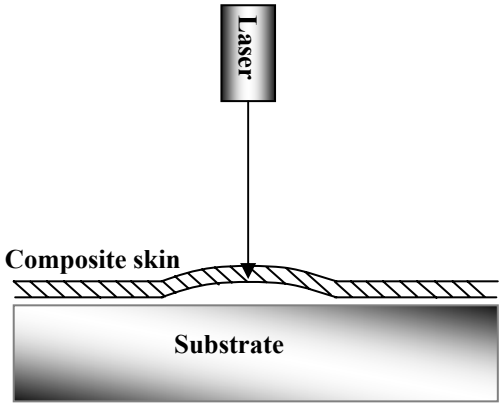

"**Fig. 1.** Thermoelastic bending."

To solve the set of equations (1), one has to set the boundary conditions. The solution for the strongly damped thermal-wave field introduces a gradient of temperature and consequently a gradient of thermal expansion (thermoelastic bending) that enables the vibration of a thin plate above a delamination at the excitation frequency (fig. 1). To attain thermoelastic bending the thickness of the plate should be much smaller than its lateral dimensions. Effects

of thermoelastic bending overshadowing the thermal dilatation have been reported before by several scientists [6, 7].
Provided that there is vibration it is straightforward to show that the temperature at the surface can be approximated by a mixture of the two components at the extremes. Consider, for instance, a delamination with an initial air gap thickness d_0 that oscillates independently at frequency ω_1. If the amplitude of the oscillation is ε, then the air gap thickness at any time t, is given by:

$$\mathrm{d}=\mathrm{d}_0+\varepsilon\sin(\omega_1 t) \tag{3}$$

The amplitude A and the phase ϕ of the thermal wave at the surface, are functions of the excitation frequency ω_2 as well as the thickness of the delamination air gap d. Their dependence can be simply calculated, e.g. considering a one-dimensional model, Thus,

$$T(t)=A(\omega_2,d)\sin(\omega_2 t+\phi(\omega_2,d)) \tag{4}$$

Substituting (3) into eq. (4), using the fact that □/d_0 is very small and expanding in Taylor series disregarding higher orders yields:

$$\begin{aligned} T(t) &= A(\omega_2,\mathrm{d}_0+\varepsilon\sin(\omega_1 t))\sin(\omega_2 t+\phi(\omega_2,\mathrm{d}_0+\varepsilon\sin(\omega_1 t))) \\ &= \left(A(\mathrm{d}_0)+\frac{\partial A}{\partial d}\varepsilon\sin(\omega_1 t)\right)\sin\left(\omega_2 t+\phi(\mathrm{d}_0)+\frac{\partial\phi}{\partial d}\varepsilon\sin(\omega_1 t)\right) \end{aligned} \tag{5}$$

Deploying the second term using well known trigonometric identities and Taylor expanding the functions of small arguments in □ gives:

$$\begin{aligned} &\sin\left(\omega_2 t+\phi(\mathrm{d}_0)+\frac{\partial\phi}{\partial d}\varepsilon\sin(\omega_1 t)\right)= \\ &=\left[\sin\left(\omega_2 t+\phi(\mathrm{d}_0)\right)\cos\left(\frac{\partial\phi}{\partial d}\varepsilon\sin(\omega_1 t)\right)+\cos\left(\omega_2 t+\phi(\mathrm{d}_0)\right)\sin\left(\frac{\partial\phi}{\partial d}\varepsilon\sin(\omega_1 t)\right)\right] \\ &=\left[\sin\left(\omega_2 t+\phi(\mathrm{d}_0)\right)\left[1-\left(\frac{\partial\phi}{\partial d}\varepsilon\sin(\omega_1 t)\right)^2\right]+\cos\left(\omega_2 t+\phi(\mathrm{d}_0)\right)\left(\frac{\partial\phi}{\partial d}\varepsilon\sin(\omega_1 t)\right)\right] \end{aligned} \tag{6}$$

Substituting back to eq.(5), performing the multiplication and recasting, results in a frequency mixing expression. Neglecting the higher orders, the expression can be written as:

$$\begin{aligned} T(t) &= A(\mathrm{d}_0)\sin\left(\omega_2 t+\phi(\mathrm{d}_0)\right)+\frac{\partial A}{\partial d}\varepsilon\sin(\omega_1 t)\sin\left(\omega_2 t+\phi(\mathrm{d}_0)\right) \\ &\quad +A(d_0)\cos\left(\omega_2 t+\phi(\mathrm{d}_0)\right)\left(\frac{\partial\phi}{\partial d}\varepsilon\sin(\omega_1 t)\right) \\ &= A(\mathrm{d}_0)\sin\left(\omega_2 t+\phi(\mathrm{d}_0)\right)-\frac{1}{2}\frac{\partial A}{\partial d}\varepsilon\left(\cos(\omega_1 t+\omega_2 t+\phi(\mathrm{d}_0))-\cos(\omega_1 t-\omega_2 t-\phi(\mathrm{d}_0))\right)+ \\ &\quad +\frac{1}{2}\frac{\partial\phi}{\partial d}\varepsilon A(d_0)\left(\sin(\omega_1 t+\omega_2 t+\phi(\mathrm{d}_0))+\sin(\omega_1 t-\omega_2 t-\phi(\mathrm{d}_0))\right) \end{aligned} \tag{7}$$

In the frequency mixing terms, the factors $\frac{\partial A}{\partial d}\varepsilon$ and $\frac{\partial\phi}{\partial d}\varepsilon$ can be expressed as follows:

$$\frac{\partial A}{\partial d}\varepsilon = \frac{A(d_0+\varepsilon/2)-A(d_0-\varepsilon/2)}{\varepsilon}\varepsilon = A(d_0+\varepsilon/2)-A(d_0-\varepsilon/2)$$
$$\frac{\partial \phi}{\partial d}\varepsilon = \frac{A(d_0+\varepsilon/2)-A(d_0-\varepsilon/2)}{\varepsilon}\varepsilon = \phi(d_0+\varepsilon/2)-\phi(d_0-\varepsilon/2) \quad (8)$$

For the case where the thickness oscillations are induced by the probing thermal wave field itself, ω_1 and ω_2 *are equal*, and equation (7) demonstrates that the temperature signal exhibits oscillation at both frequencies ω and 2ω. The amplitude and phase of the second harmonic are provided by the difference in the characteristic values for the two extremes of the vibration.

3. EXPERIMENTAL SETUP

The experimental setup, shown in Figure 2, consists of a diode pumped solid-state laser (DPSS, Λ=532 nm) intensity modulated by an acousto-optic modulator (IntraAction), a lens, the position of which controls the spot size of the laser beam, the computer controlled 3D stage for supporting and positioning the sample, and an infrared detector. A germanium window with a transmission bandwidth of 2-14 μm is mounted in front of the detector to block any visible radiation from the pump laser. The infrared emission from the sample is collected and focused to a liquid N_2 cooled HgCdTe (MCT) detector (bandwidth 2-12 microns and sensing area 0.05 x 0.05 mm) using two 90-degree offaxis gold-coated paraboloidal mirrors. The signal from the detector is amplified and fed to a lock-in-amplifier (SR 830). The sample is positioned on the horizontal plane on a three-dimensional translation stage in order to allow adjusting the distance at the focus of the parabolic mirror as well as performing the area scans.

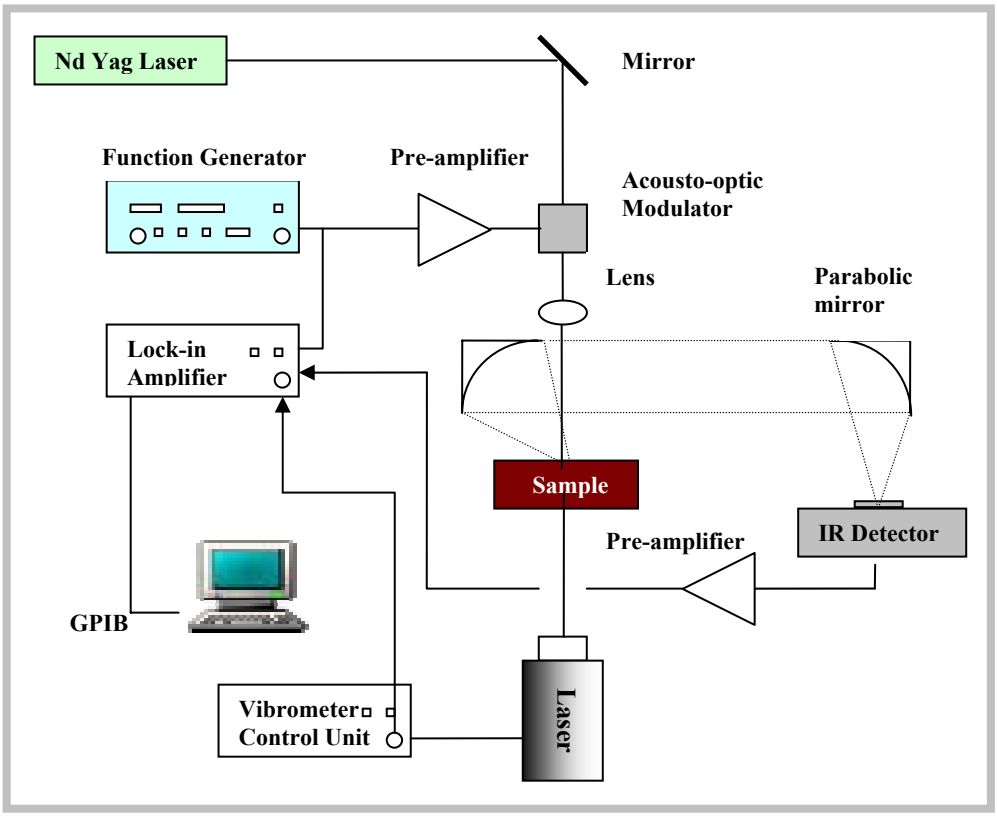

"**Fig. 2.** Experimental setup for IR photothermal radiometry."

The same setup was also used to measure the displacement field at the surface of a thin circular layer of the carbon/epoxy sample. To perform such a measurement, in order to retain the signal of the Doppler laser, the latter as well as the sample were held fixed. Instead, the excitation laser beam was scanning in a raster-like manner through a lens which was placed on an X-Y translation stage moving laterally to the horizontal plane.
The control of the position of the sample in each case as well as the excitation frequency and the data acquisition were automated.

4. SAMPLE PREPARATION

In order to perform the measurements using the aforementioned different techniques, two samples were manufactured, which are depicted in figure 3. A cross-ply laminate was prepared consisting of carbon fibre reinforced epoxy resin (prepreg fibredux 920). A hole (diameter 6mm) was opened with the milling machine reducing the thickness to a thin layer of 180μm. Then a mushroom-like aluminium piece was made to fit exactly inside the hole. The two pieces enabled, using different spacers, to control the air gap in between the thin composite layer and the metallic substrate (fig 3). The former piece of Carbon/Epoxy was also used to measure the displacement field in different excitation frequencies over the thin layer with the Doppler method as it was loaded with a laser beam from the rear side.

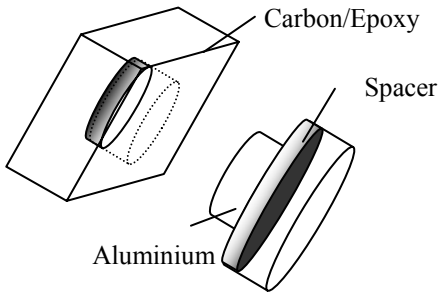

"**Fig. 3.** Carbon/Epoxy sample and matching mushroom-like aluminium piece."

5. RESULTS & DISCUSSION

a. Laser vibrometer method

The Laser vibrometer method was used to measure the displacement of the thin layer above the delamination as it was excited by the laser beam. This offers a quantitative indication for the source of the second harmonic generation due to the thermoelastic bending effect. Knowing the bending displacement caused, one can estimate the order of the second harmonic component using equation (8) and theoretical simulations. Measurements were performed with the excitation both from the front as well as the rear side of the sample positioned laterally to the horizontal plane giving the same results. At this point it should be stressed that even though the method used gives a good estimate for the order of the bending displacement there are uncertainties regarding two points. The first one concerns the change of the position of the application of the bending moment as the laser beam scans and the second one is associated with the possible excitation around a centre that is not the centre of the circular plate. Nevertheless, this indirect method was sufficiently adequate to provide the aforementioned estimation as well as a view of the thermal anisotropy since, at low frequencies, the displacement and the thermal-wave field are pretty much equivalent. Figure 4 shows the displacement field around the excitation laser beam. The maximum displacement

amplitude peak-to-peak ε stays below 300*nm* at 1Hz for the experimental parameters under consideration.

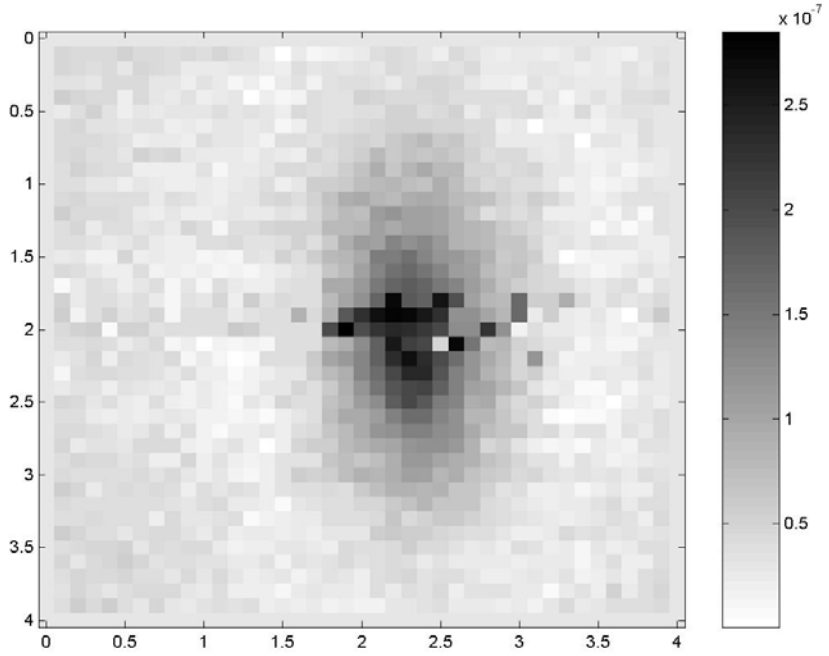

"**Fig. 4.** Area (4mm x 4mm) scan over a circular (d=6mm) thin (200μm) layer of Carbon/Epoxy excited with a focused laser beam (D=1mm) at 1Hz with the Laser vibrometer method."

After an area scan at 300Hz, to optimise the signal of vibrometer, the beams were aligned to the position of the maximum displacement in order to perform a frequency scan and evaluate the influence of the frequency on the bending displacement. This scan is depicted in figure 5. The phase instability at about 40Hz does not originate from resonance [10] but rather from the electronic noise.

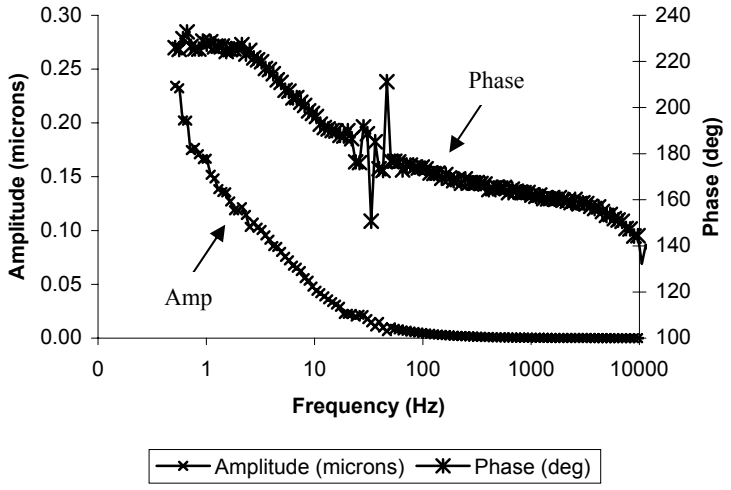

"**Fig. 5.** Frequency scan over a circular (d=6mm) thin (200μm) layer of Carbon/Epoxy excited with a focused laser beam (D=1mm) with respect to displacement (Laser vibrometer method)."

b. Theoretical simulations of the second harmonic signal

In this section, theoretical simulations of the second harmonic are presented based on eq. (8) and on airgap thickness varitations of the order of the experimentally observed one. The thermal-wave field is determined for static cases of various delamination air gaps $d_0 \pm \varepsilon/2$ and the overtone is calculated from the difference in their characteristic values based on a one-dimensional model. The thermal properties of all the materials used are presented in Table 1 [2, 9, 11].

"**Table 1.** Thermal properties of materials used."

Property / Material	Density (Kg/m^3)	Thermal Conductivity (W/m.K)	Specific Heat (J/Kg.K)	Thermal Diffusivity (m^2/sec)	Thermal Effusivity ($W.s^{1/2}/m^2.K$)	TW interfacial coupling coef. with air
Air	1.16	0.026	1007	$2.23e^{-5}$	5.511	-
Aluminium	2700	238	945	$9.1e^{-5}$	23688	4471
Carbon/Epoxy ($\perp$)	1550	0.56835	793.7	$4.62e^{-7}$	836	151

The thermal-wave interfacial coupling coefficient quantifies the degree of thermal inhomogeneity across the boundary planes (ratio of thermal impedances) and reduces to an effusivity ratio in the one-dimensional case. This coefficient prescribes the contrast in the presence of a defect or any interface.

One of the techniques that could be exploited for the detection of overtones is the photothermal deflection technique using the 'mirage' effect. Therefore, the simulations were adapted to estimate the temperature field values at a distance of 50μm away from the surface. A rival nonlinear effect in using the mirage technique is that the distance of the probe beam with respect to the surface of the sample is also oscillating due to thermoelastic bending. This variation was examined and its contribution was compared with the effect of interest.

In figure 6, results are depicted for different initial air gap sizes and for different oscillation amplitudes based on a one-dimensional model. It is clear in the first graph (fig. 6.a) that the larger the oscillation and the smaller the initial air gap entail the greater the overtone amplitude (roughly quadratic dependence). Likewise, it is apparent in the phase graphs (fig. 6.b) that the contrast (dip) becomes sharper when the oscillation amplitude is larger. It is also observed that the dip moves to the right for smaller initial air gaps.

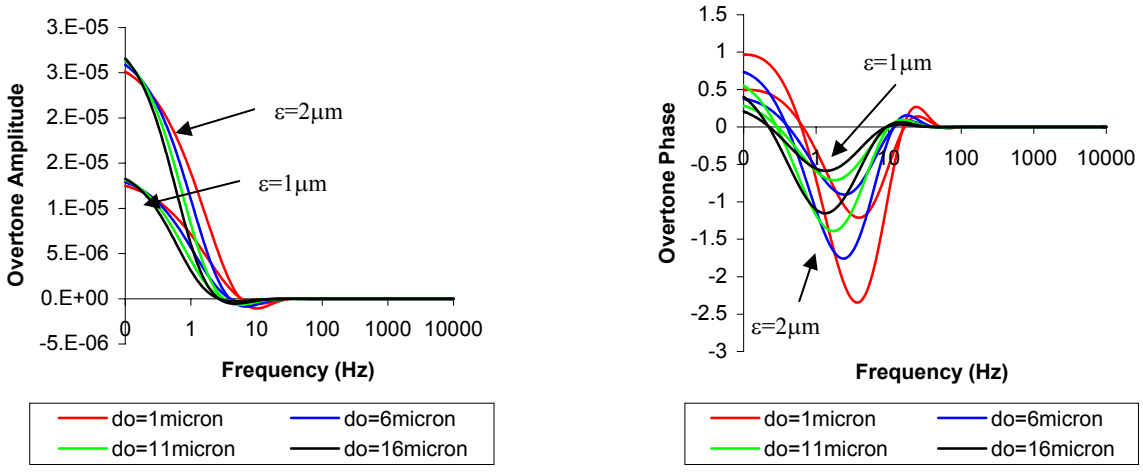

(a) (b)

"**Fig. 6.** Theoretical simulations of the overtone generation as a result of defect (under a thin layer 180 μm) size oscillation for a Carbon/Epoxy plate excited with a laser beam for various initial air gaps d_0 and oscillation amplitudes ε : (a) amplitude and (b) phase."

The next study case involved variation of the oscillation amplitude as a function of frequency as demonstrated by the use of the laser vibrometer method. So, the amplitude of the oscillation was not held constant but it was provided by the real measurements as a function of frequency. The results are shown in figure 7 for different initial air gaps. It is again apparent that the second harmonic is less strong as the initial gap increases. The frequency has to be lower so as to enable the thermal wave to probe the whole air gap and sense differences in its size. Therefore, the extreme values in the phase graph move to the left with increase of d_0.

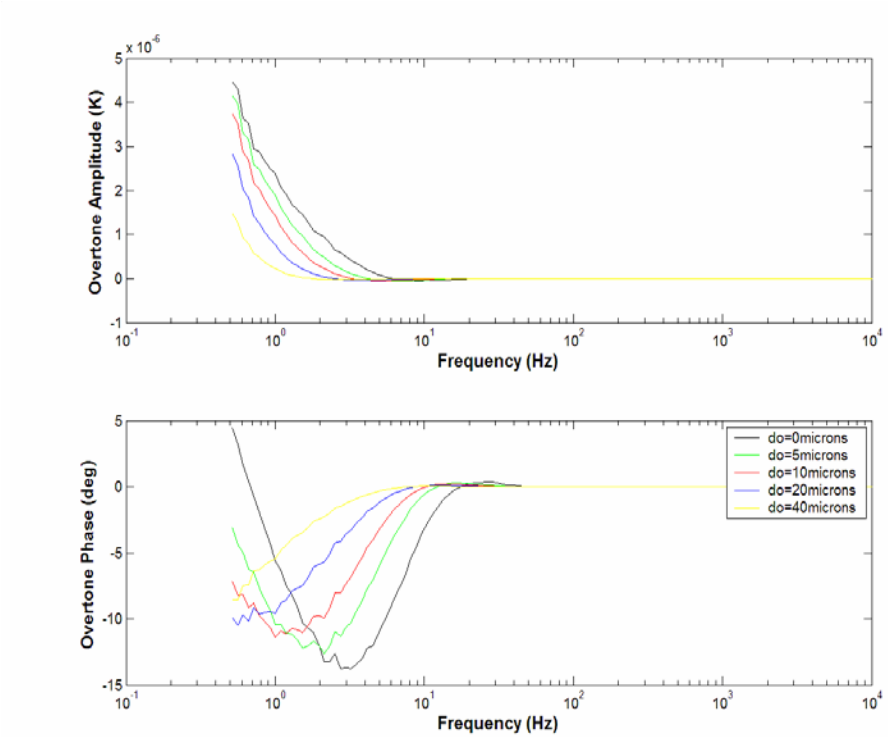

"**Fig. 7.** Theoretical simulations of the overtone generation as a result of defect (under a thin layer 180 μm) size oscillation for a Carbon/Epoxy plate excited with a laser beam for various initial air gaps and oscillation amplitudes measured with the laser vibrometer method."

Finally, the overtone generated by the vibration of the thin layer was compared with the effect of the oscillation of the probing distance when using the optical deflection technique by means of the 'mirage' effect. In figure 8, the ratio of the relative contribution is drawn as a function of frequency. It is demonstrated, thus, that for the region of interest the defect size effect is dominant, even with large amplitudes of oscillation, with one or two orders of magnitude stronger contribution to nonlinearity.

c. Fitting using Infrared photothermal radiometry

In this last section, infrared photothermal radiometry was used in order to fit experimental data with theoretical curves for the fundamental component. The aim was to demonstrate in this way that, as it was predicted in the previous sections, the defect size has a large influence on the temperature signal and therefore any considerable vibration would cause a measurable overtone. For this experimental part the sample depicted in figure 3 together with the mushroom-like aluminium part were used. The distance of the air gap between the thin composite layer and the metallic substrate was controlled with different spacers. Due to roughness inside the hollow part as well as possible inaccuracies in the thickness of the spacers, the actual distances as well as the thermal properties of the composite material were used as fitting parameters.

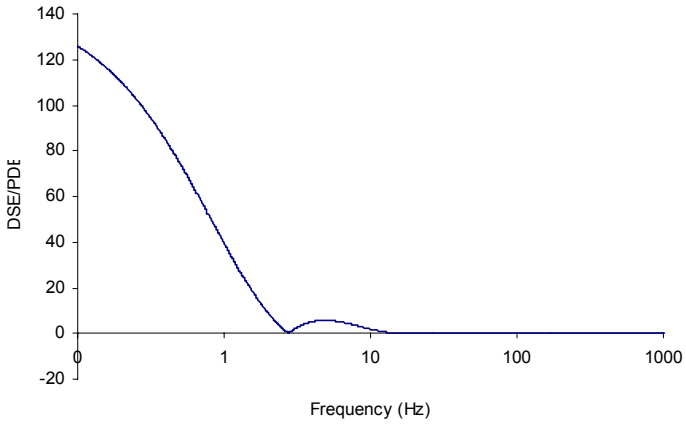

"**Fig. 8.** The ratio of DSE (Defect Size Effect) with PDE (Probing Distance Effect) as a function of frequency for amplitude of oscillation equal to 5μm."

The result is shown in figure 9. The fitting parameters as well as the error analysis on the air gap thickness are given in Table 2. The value for the thermal diffusivity is in good agreement with the initial value referenced in Table 1. Thermal conductivity, however, seems to be rather higher. This might originate from a probable high local content of carbon fibers in the particular area of the thin layer examined. The non-convergence towards the higher frequencies could be explained taking into account the scattering due to roughness.

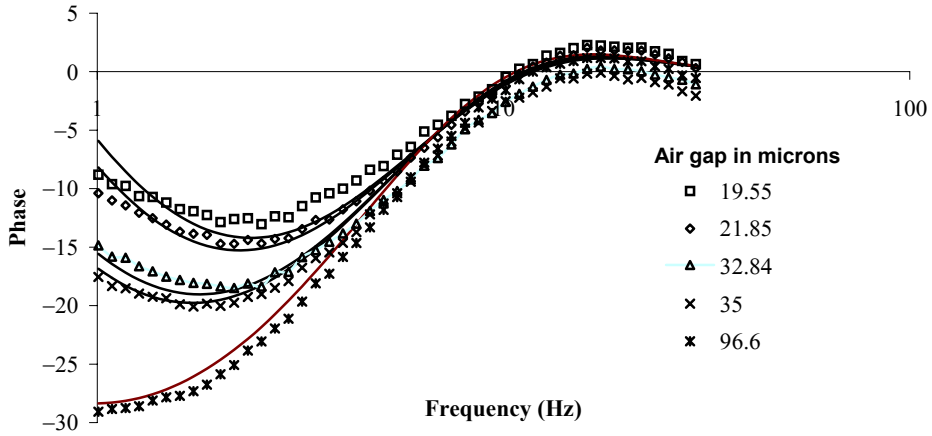

"**Fig. 9.** Fitted photothermal experimental data of a carbon/epoxy sample with various delamination openings."

"**Table 2.** Error analysis on the air gap thickness and fitting parameters."

Air gap (μm)	Fitting parameters	
19.55 ± 0.63		
21.85 ± 1.19	Thermal Diffusivity (m^2/sec)	$4.56e^{-7}$
32.84 ± 3.87	Thermal Conductivity (W/m.K)	0.722
35 ± 1.06	Layer thickness (μm)	185
96.6 ± 7.6		

6. CONCLUSIONS

The potential of nonlinear photothermal radiometry for the detection of delaminations in composite materials was confirmed. A theoretical model was developed that demonstrated what could be the effect of the oscillation of the defect size on the photothermal signal. Theoretical simulations based on real measurements using the laser vibrometer method showed that the contrast created could be exploited for the defect detection. Moreover, experimental work with infrared photothermal radiometry confirmed the effect of the defect size variation.

ACKNOWLEDGEMENTS

The authors would like to acknowledge the support of Fund of the Scientific Research - Flanders (Belgium), which made this work possible.

References

1. **Gusev, V.**, **Mandelis, A.** & **Bleiss R.** "Theory of Second Harmonic Thermal-Wave Generation: One-Dimensional Geometry", *Int. J. Therm.* **14**/2 (1992), 321-337.
2. **Kalogiannakis G.**, **Van Hemelrijck D.** & **Van Assche G.** "Measurements of thermal properties of Carbon/Epoxy and Glass/Epoxy using Modulated Temperature Differential Scanning Calorimetry", J.Comp. Mater. **38**/2 (2004), p. 163-175.
3. **Kalogiannakis, G.**, **Van Hemelrijck, D.** "Contrast enhancement of Nonlinear Photothermal Radiometry in composite materials". *Proc. 3rd Int. Conf. on Emerging Technologies in NDT,* Thessaloniki, 26-28 May 2003.
4. **Gusev, V.**, **Mandelis, A.** & **Bleiss R.** "Theory of Strong Photothermal Nonlinearity from Sub-Surface Non-Stationary ("Breathing") Cracks in Solids". *J. Appl. Phys.* **A57**: 229-233 (1992).
5. **Mandelis, A.**, **Salnick, A.**, **Opsal, J.** & **Rosencwaig, A.** "Nonlinear fundamental thermal response in three-dimensional geometry: Theoretical model", *J. Appl. Phys.* **85**/3 (1999), 1811-1821.
6. **Cielo, P.**, **Maldague, X.**, **Rousset, G.** & **Jen, CK.** "Thermoelastic inspection of layered materials: dynamic analysis". *Mater. Eval.* **43**/9, 1111-1116 (1985).
7. **Rajakarunanayake, Y.N.** & **Wickramasinghe, H.K.** *Appl. Phys. Lett.* **48,** 218 (1986)
8. **Nowacki W.** "Thermoelasticity", Pergamon Press, ISBN 0-08-024767-9 (1986)
9. **Almond D., Patel P.,** "Photothermal Science and Techniques", Chapman and Hall, London (1996)
10. **Roark R.J. & Young W.C.** "Formulas for Stress and Strain", Mc Graw Hill Book Company, ISBN 0-07-053031-9
11. **Lauriks W., Desmet C., Glorieux C. & Thoen J.** "Investigation of the thermal anisotropy of unidirectional carbon fiber reinforced composite plates using optically generated thermal waves and a noncontact optical detection technique" *J. Mater. Res.* **8**/12 (1993)